The EEG microstate topography is predominantly determined by intracortical sources in the alpha band

Milz, P ; Pascual-Marqui, R D ; Achermann, P ; Kochi, K ; Faber, P L

DOI: https://doi.org/10.1016/j.neuroimage.2017.08.058

Accepted Manuscript

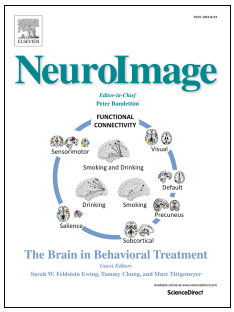

The EEG microstate topography is predominantly determined by intracortical sources in the alpha band

P. Milz, R.D. Pascual-Marqui, P. Achermann, K. Kochi, P.L. Faber

PII: S1053-8119(17)30705-X

DOI: 10.1016/j.neuroimage.2017.08.058

Reference: YNIMG 14289

To appear in: *NeuroImage*

Received Date: 21 April 2017

Revised Date: 1053-8119 1053-8119

Accepted Date: 23 August 2017

Please cite this article as: Milz, P., Pascual-Marqui, R.D., Achermann, P., Kochi, K., Faber, P.L., The EEG microstate topography is predominantly determined by intracortical sources in the alpha band, *NeuroImage* (2017), doi: 10.1016/j.neuroimage.2017.08.058.

The EEG microstate topography is predominantly determined by intracortical sources in the alpha band

P. Milz, R.D. Pascual-Marqui, P. Achermann, K. Kochi, P.L. Faber

The KEY Institute for Brain-Mind Research, Department of Psychiatry, Psychotherapy and Psychosomatics, University Hospital of Psychiatry, P.O. Box 1931, CH-8032 Zurich, Switzerland.

Mailing address: The KEY Institute for Brain-Mind Research, University Hospital of Psychiatry, PO Box 1931, CH-8032 Zurich, Switzerland

E-Mail addresses authors: patricia.milz@key.uzh.ch, pascualm@key.uzh.ch, acherman@uzh.ch, osakachochiku@gmail.com, pfaber@key.uzh.ch

Corresponding author: Patricia Milz, The KEY Institute for Brain-Mind Research, University Hospital of Psychiatry, PO Box 1931, CH-8032 Zurich, Switzerland, phone: 0041445005349

Abstract

Human brain electric activity can be measured at high temporal and fairly good spatial resolution via electroencephalography (EEG). The EEG microstate analysis is an increasingly popular method used to investigate this activity at a millisecond resolution by segmenting it into quasi-stable states of approximately 100 ms duration. These so-called EEG microstates were postulated to represent atoms of thoughts and emotions and can be classified into four classes of topographies A through D, which explain up to 90 % of the variance of continuous EEG. The present study investigated whether these topographies are primarily driven by alpha activity originating from the posterior cingulate cortex (all topographies), left and right posterior cortices, and the anterior cingulate cortex (topographies A, B, and C, respectively).

We analyzed two 64-channel resting state EEG datasets (N=61 and N=78) of healthy participants. Sources of head-surface signals were determined via exact low resolution electromagnetic tomography (eLORETA). The Hilbert transformation was applied to identify instantaneous source strength of four EEG frequency bands (delta through beta). These source strength values were averaged for each participant across time periods belonging to a particular microstate. For each dataset, these averages of the different microstate classes were compared for each voxel. Consistent differences across datasets were identified via a conjunction analysis.

The intracortical strength and spatial distribution of alpha band activity mainly determined whether a head-surface topography of EEG microstate class A, B, C, or D was induced. EEG microstate class C was characterized by stronger alpha activity compared to all other classes in large portions of the cortex. Class A was associated with stronger left posterior alpha activity than classes B and D, and class B was associated with stronger right posterior alpha activity than A and D.

Previous results indicated that EEG microstate dynamics reflect a fundamental mechanism of the human brain that is altered in different mental states in health and disease. They are characterized by systematic transitions between four head-surface topographies, the EEG microstate classes. Our results show that intra-cortical alpha oscillations, which likely reflect decreased cortical excitability, primarily account for the emergence of these classes. We suggest that microstate class dynamics reflect transitions between four global attractor states that are characterized by selective inhibition of specific intra-cortical regions.

Keywords

EEG, microstates, LORETA, source localization, functional significance, default mode network

1. Introduction

Human brain electric activity can be obtained at a high temporal and at a fairly good spatial resolution via electroencephalography (EEG). Continuous EEG data may be analyzed based on a wide range of methods. The EEG microstate analysis has gained increasing popularity (Khanna et al., 2015; Koenig and Brandeis, 2016; Mégevand et al., 2008; Pedroni et al., 2016; Pipinis et al., 2016) in recent years. It is particularly attractive for the investigation of cognitive and emotional brain processes (Lehmann, 1990) since it can identify discontinuous, non-linear changes of global functional brain states at a very high temporal resolution (e.g. Lehmann et al., 1987; Lehmann et al., 2010).

The EEG microstate analysis inspects the topography of the head-surface potential changes of brain electric activity at a millisecond resolution (Koenig et al., 2002). This procedure has already yielded fundamental insights into human brain functioning. Firstly, it revealed that the brain's electric activity distribution does not change continuously with time, but in discrete steps. One head-surface topography does not transform smoothly into another but stays quasi-stable for a period of approximately 80-120 ms and then abruptly changes to another topography (Lehmann et al., 1987; Lehmann et al., 2009; Lehmann and Skrandies, 1980; Michel et al., 2009). Secondly, it revealed that up to 90 % of the variance of the electric potential changes identified via EEG during eyes closed resting can be explained by transitions between only four head-surface topographies (Khanna et al., 2014; Koenig et al., 2002; Wackermann et

al., 1993). These four primary head-surface topographies may represent global brain electric attractor states that the brain transitions into systematically in any individual.

These four characteristic EEG topographies have been extracted consistently across studies via different procedures and clustering algorithms (e.g. Khanna et al., 2014; Pascual-Marqui et al., 2014; Pascual-Marqui et al., 1995). By convention, the four topographies were labeled EEG microstate classes A to D (Koenig et al., 2002, see Figure 1). They were remarkably similar in health and disease, different age groups, and during different mental states (resting, task, sleep) (Britz et al., 2010; Brodbeck et al., 2012; Faber et al., 2014; Kindler et al., 2011; Koenig et al., 2002; Milz et al., 2016a; Schlegel et al., 2012).

---------- *Figure 1 about here* ----------

However, unlike the topography, the occurrence, frequency, and sequential order of these EEG microstate classes profoundly varied in different populations and mental states. For example, microstate class A was more, class D less prominent in patients and risk groups of several mental disorders compared to healthy controls (Andreou et al., 2014; Faber et al., in preparation; Koenig, 2016; Koenig et al., 1999; Lehmann et al., 2005; Milz, 2016; Nishida et al., 2013; Rieger et al., 2016; Strelets et al., 2003; Tomescu et al., 2014). The length of microstate classes A and B shortened and the occurrence of class C increased with age in the awake eyes closed resting state (Koenig et al., 2002). The mean duration of all classes was lengthened during deep sleep (Brodbeck et al., 2012). Class B duration was longer during meditation (Faber et al., 2005) and healthy controls showed a preferred microstate sequence (A-C-D-A) that was reversed in schizophrenic patients (A-D-C-A) (Lehmann et al., 2005).

Apparently, several EEG microstate parameters are consistently altered in particular populations and particular mental states. However, the functional interpretation of these alterations has proven difficult. Based on their unique properties, the EEG microstates have been postulated to represent the atoms of thoughts and emotions (Lehmann, 1993). However, so far no conclusive functional implications can be made on what it means when the occurrence and / or the duration of the microstates of a particular class are altered. The functional significance, that is the mental process the EEG microstate classes and their concatenations relate to, has been addressed in previous studies, but has not yet been clearly established (Britz et al., 2010; Milz et al., 2016a; Seitzman et al., 2016).

A promising approach to learn more about the functional significance of the EEG microstate classes in the brain is to identify and infer potential functions from their cortical sources. The cortical sources of head-

surface recorded EEG can be identified via source localization algorithms such as exact Low Resolution Electromagnetic Tomography (eLORETA: Pascual-Marqui, 2007). A previous study applied this approach to EEG microstate class topographies computed based on a broad band of 2-20 Hz (Pascual-Marqui et al., 2014). It revealed that the four EEG microstate classes have a common source in the posterior cingulate and additional sources in the left occipital/parietal, right occipital/parietal, and anterior cingulate cortices for microstate classes A through C, respectively (Pascual-Marqui et al., 2014). These sources corresponded to the four main hubs of the metabolic default mode network (Raichle et al., 2001).

Thus, it was suggested that the default mode network may not be characterized by simultaneous activity in different brain regions but temporally distinct activations of different network components that are blurred by the low temporal resolution in fMRI (Pascual-Marqui et al., 2014). Consequently, the temporal dynamics of the four EEG microstate classes might reflect a high-level brain process that activates and / or deactivates these four default mode network hubs repeatedly with various durations, frequency, and in different sequences. Moreover, the large proportion of variance explained by the four microstate classes suggests that this dynamic may be the most prominent component of brain electric activity as measured via continuous EEG recordings altogether.

However, two important pieces of information cannot be derived from the above study. Firstly, it remains unclear whether the microstate class transitions reflect systematic sequences of activation and/or deactivation of these default mode network hubs. Secondly, it remains unclear whether the microstate classes are solely driven by the reported sources or whether additional sources contribute that may or may not systematically differ between classes.

The first point relates to the question whether the cortical activity distributions that give rise to the four microstate class topographies rely on excitatory or inhibitory brain electric activity or a combination of the two. It has been argued that it may be alpha band activity that predominantly establishes the microstate topographies (Milz et al., 2016a) since the alpha band (8.5-12 Hz) is the EEG frequency band of strongest power in the range of 2-20 Hz, which is the frequency range conventionally used to compute the EEG microstates (Koenig et al., 2002; Lehmann et al., 2005; Pascual-Marqui et al., 2014). However, the alpha band may primarily reflect inhibitory rather than excitatory functions, particularly in task-related brain areas (Milz et al., 2016a; Milz et al., 2016b; Pfurtscheller, 2003; Salenius et al., 1995; Slatter, 1960).

Previous studies revealed no conclusive results concerning the association of the four EEG microstate classes with specific power spectral distributions (Britz et al., 2010; Musso et al., 2010). However, these studies investigated mean spectra across all channels that may disguise potential channel-location-specific

associations. To our knowledge, no previous study investigated head-surface localization- or source-dependent power effects on the occurrence of the EEG microstate classes.

The second point relates to the question whether the default mode network hubs, which were identified as a simple average of the sources corresponding to the set of topographic maps of the same microstate state class (Pascual-Marqui et al., 2014), are indeed uniquely involved in the generation of the microstate class topographies. It is possible that weaker sources outside the default mode network exist, which were masked by the gross averaging procedure. Such weaker sources could likely be identified by comparing source strengths between the generators which establish the different EEG microstate class topographies.

The difficulty with associating the EEG microstate classes with EEG frequency bands is the different time scales (different temporal resolution) required to identify them. For each measured sampling point, the one of the four EEG microstate classes that it belongs to can be determined based on minimal dissimilarity. However, traditional frequency domain analysis techniques, which are used to compute the EEG power in a particular frequency band, require longer time periods than just a few milliseconds. Fortunately, this problem can be overcome by means of a different type of method that is used in the field of time-frequency analysis, the discrete Hilbert transform. By means of the Hilbert transform, the time varying instantaneous amplitude of a signal, corresponding to a specified frequency band, can be computed as the envelope of the analytic signal (Marple, 1999; Poularikas, 1998). Thus, with this method, we are able to retrieve for each frequency band and voxel the source strength at each time frame (sample) which can be associated with the corresponding microstate.

In the present study, we identified the frequency-dependent cortical sources of the four EEG microstate classes in two independent EEG datasets recorded in healthy individuals during eyes closed resting (N=61 and N=78). This was achieved by applying the Hilbert transform to eLORETA (Pascual-Marqui, 2007) time series of cortical current density estimates in 6239 cortical voxels, calculated from the EEG recordings. In this manner, for each individual, average frequency-dependent source strengths were computed across all available EEG time frames which induced a class A, B, C, or D head-surface topography, respectively. These frequency-dependent source distributions were then compared via paired t-tests between microstate classes for each dataset. A conjunction analysis revealed the most consistently deviant sources of activity between classes across the two datasets.

We hypothesized that the alpha frequency band determines whether a head-surface topography of class A, B, C, or D is induced (as suggested by Milz et al., 2016a). Therefore, we expected differences in source strength between the four EEG microstate classes to be more prominent in the alpha band than in the other bands. Based on the primary sources of the microstate classes identified by Pascual-Marqui et al.

(2014), we hypothesized alpha source strength to be strongest in the left posterior, right posterior, and the anterior cingulate cortices for microstate classes A, B, and C, respectively when compared to the other classes.

2. Material and methods

2.1 Datasets and preprocessing

Two preprocessed independent datasets (Dataset 1 and Dataset 2) were available for analysis. They both comprise continuous EEG recordings from healthy participants during eyes closed resting. Dataset 1 comprises 61-channel EEG data from 61 male participants (aged: 18-34 years) during 7 resting runs of 50 s duration each. This dataset was recorded at the KEY Brain Mapping Laboratory at the University Hospital of Psychiatry, Zurich, using a 64-channel BioSemi Recording System (see Milz et al., 2016a for a detailed description). Dataset 2 comprises 1-min, 61-channel eyes closed resting EEG data from 78 participants. This dataset is a subset of freely available EEG recordings from the internet (https://physionet.org/physiobank/database/eegmmidb/). All technical details about these recordings and their preprocessing are described in Goldberger et al. (2000), Pascual-Marqui et al. (2014), and Schalk et al. (2004). For maximal comparability and to avoid effects of intermittent conditions, only the first resting run of Dataset 1 was used for the analysis.

Datasets 1 and 2 were originally recorded with 64 channels at the following positions: Fp1/2, Fpz, AF7/8, AF3/4, AFz, F7/8, F5/6, F3/4, F1/2, Fz, FT7/8, FC5/6, FC3/4, FC1/2, FCz, T7/8, C5/6, C3/4, C1/2, Cz, TP7/8, CP5/6, CP3/4, CP1/2, CPz, P7/8, P5/6, P3/4, P1/2, Pz, PO7/8, PO3/4, POz, O1/2, Oz, P9/10, and Iz (according to the International "10-10 System": Chatrian et al., 1985; Nuwer, 1987). For analysis, three of the 64 channels (P9, P10, and Iz) were discarded since they were significantly more distant from the corresponding closest neighbor compared to all closest neighbor inter-distances. This resulted in a more uniform spatial sampling of the scalp with the remaining 61 non-outlier electrodes (see also Milz et al., 2016a; Pascual-Marqui et al., 2014). Original sampling rates were 2048 Hz and 160 Hz, for datasets 1 and 2 respectively. For dataset 1, preprocessing included resampling to 256 Hz and the extraction of artefact-free 2-s epochs. For dataset 2, no resampling was done and 1-s epochs were extracted from the available 1-min of artefact-free EEG.

In sum, for the two datasets 5828 s of EEG were available during the first eyes closed resting run (Dataset 1: 1382 s, Dataset 2: 4446 s). As commonly done for EEG microstate analysis, datasets were filtered between 2-20 Hz prior to analysis and re-referenced to average reference (Koenig et al., 2002; Lehmann et al., 2005; Pascual-Marqui et al., 2014). This was possible since the EEG devices used to record both datasets used amplifier filter settings that included this common broad band for analysis.

2.2 Microstate analysis

EEG microstate analysis was performed separately for each dataset with *keypy*. Keypy is an open source library for EEG microstate analysis (Milz, 2016; Milz et al., 2016a) and freely available from: www.github.com/keyinst/keypy. It is scriptable and thus requires no direct interaction via a graphical user interface.

EEG microstate segmentation was performed based on the four normative microstate class topographies published by Koenig et al. (2002) (see Figure 1). For each participant and each epoch, the time segments corresponding to a particular class of the four EEG microstate topographies were identified. This was done by extracting all global field power (GFP) peaks within a given epoch (see also e.g. Andreou et al., 2014; Katayama et al., 2007; Schlegel et al., 2012). The EEG topography at each GFP peak was then labeled A, B, C, or D based on their minimal topographical dissimilarity (Lehmann and Skrandies, 1980) with the four normative maps (disregarding polarity). Microstate beginning and endpoints were defined as the midpoint between two GFP peaks attributed to two different classes. Within each 2-s epoch, the beginning of the first and the end of the last microstate cannot be determined and thus the respective time segments were excluded from the subsequent analysis (see also Milz et al., 2016a). Note that the approach of identifying microstates based on GFP peaks has the advantage that topographies with a poor signal to noise ratio can be disregarded for microstate segmentation. In sum, we applied the same algorithm that has been used previously (e.g. Koenig et al 2002, Koenig et al 1999, Pascual-Marqui et al 1995) with two modifications: (1) we identified the time segments corresponding to a particular microstate based on the four classes previously described in the literature rather than extracted via a data-driven manner and (2) the first and last EEG microstate of the 2-s epochs were not considered as applied by Milz et al., 2016a.

2.3 Frequency-dependent intra-cortical source activities

Frequency-dependent intra-cortical instantaneous amplitudes were computed separately for each dataset as follows.

In a first step, for each EEG recording, time series of electric neuronal activity were computed with exact low resolution electromagnetic tomography (eLORETA: Pascual-Marqui, 2007). In the next step, by means of the Hilbert transform, band limited instantaneous amplitude of the source signals (i.e. envelopes) were computed at each cortical voxel. In particular, for each time frame, the instantaneous amplitude signals (source strength) at 6239 cortical voxels were computed for four frequency bands: delta: 2-6 Hz, theta: 6.5-8 Hz, alpha: 8.5-12 Hz, and beta: 12.5-20 Hz (see Kubicki et al., 1979; Niedermeyer and da Silva, 2005). Note that relatively broad frequency bands were used, without subdividing the alpha and beta bands, in order to ensure that the analytic signals retained high degrees of

freedom (i.e. that they were not limited to near single frequency sine waves). We further note that the instantaneous amplitudes can be calculated by techniques other than the Hilbert transform, such as the short-time Fourier transform or by means of certain wavelets. However, all these methods should reveal similar results, since they are essentially equivalent (see e.g. Bruns, 2004).

Thus, this procedure results at each voxel and for each frequency band in four time varying signals of instantaneous source strength. More importantly, from another point of view, this procedure reveals for each time frame, images of the instantaneous strength of cortical generators of the different oscillatory activities (delta, theta, alpha, and beta). This time-varying frequency decomposition allows for the first time, to perform an appropriate association with the corresponding microstate classes.

It is important to note that the instantaneous amplitude of the different frequency bands of the EEG (and of the eLORETA source signals) are, by definition, relatively slow signals, since they correspond to the "envelopes" of the oscillatory activity. In terms of time resolution, these slow changing signals are compatible with the dynamics of microstate class signals, where a microstate has a duration of approximately 100 ms. These observations support the use of the methods of analysis developed here for the frequency decomposition of the EEG microstates.

2.4 Statistics

For the four EEG microstate classes, their intra-cortical sources corresponding to each frequency band were identified separately for each dataset as follows. For each participant, the time frames associated with microstate classes A, B, C, and D were determined (as described above). Next, for each participant, for each frequency band, and each voxel, the eLORETA instantaneous amplitude values attributed to a particular class were averaged across all time frames. Thus, this procedure yielded a total of 16 mean intra-cortical source distributions for each participant, consisting of each of the four microstate classes, decomposed by frequency bands (four in total). For each frequency band and each voxel, the cortical instantaneous amplitudes of all possible pairs of classes were compared. Paired t-test results were combined between datasets via a conjunction analysis. Conjoint significance across two independent tests (Friston et al., 1999; Nichols et al., 2005) is achieved when the maximum of the two-tailed p-value of a given voxel and frequency band is smaller than the square root of the specified significance level (in our case uncorrected 0.001, i.e., both voxels must satisfy $p < 0.0316$, see also Friston et al., 1999). We note that in our datasets, the p-value of 0.001 corresponded to a t-value of 3.4602 for our dataset 1, and 3.4214 for dataset 2. These values were comparable to the t-values retrieved for conventional $p<.05$ and $p<.10$ thresholds when computationally-expensive corrections for multiple testing were applied via the very conservative non-parametric permutation test implemented in LORETA (e.g. the mean corrected t-

thresholds for dataset 2 for the critical alpha band were 3.549 and 3.305 for $p<.05$ and $p<.10$, respectively), which relies on the max t-value statistic (Nichols and Holmes, 2002).

2.5 Gravity centers and region of interest-based means of intracortical source activities in the alpha band

Differences in source strength between classes were dominated by the alpha band. For this band, two additional analyses were computed: a gravity center analysis and a region of interest (ROI) analysis.

The gravity center analysis was used to identify the core of the complex spatially-distributed source activity pattern revealed by eLORETA. This method reduces the multivoxel data in a functionally meaningful way, in that it assesses the principal aspects of the spatial organization of brain electric activity. Even though, we cannot directly infer from this analysis that the gravity center itself must have been the source of strongest activity, different gravity centers must result from different spatial organizations of activated neuronal populations (see also Tsuno et al., 2002). For each EEG microstate class, the cortical 3D coordinates of the center of gravity of the mean source activity distribution across participants and across voxels was computed. The gravity center is defined as the weighted average coordinates with the weights given by the mean instantaneous amplitudes.

The ROI analysis was computed as follows. After the main analysis, nine clusters of voxels turned out to differ in source strength between the four EEG microstate classes. Some of these differences were increases others were decreases of activity from one class to another. Each of these nine clusters was defined as one ROI. Subsequently, for each of the two datasets, and each of these nine ROIs, the mean source strength across all voxels within a ROI, was computed. Mean absolute source strengths within these ROIs across participants are reported and comparisons between ROIs within classes were performed by paired t-tests.

3. Results

3.1 Explained variance of EEG microstate class topographies and descriptive parameters

For Dataset 1, the four normative EEG microstate classes explained on average across participants 76 % of the variance of all global field power peaks and 70 % of the variance of all EEG time frames. For Dataset 2, the four normative EEG microstate classes explained on average across participants 72 % of the variance of all global field power peaks and 65 % of the variance of all EEG time frames. The average time spent in the four classes (mean duration), their mean occurrence per second (mean occurrence), and the mean percentage of time they covered (coverage) across participants can be found in Inline Supplementary Table 1.

---------- *Inline Supplementary Table 1 about here* ----------

3.2 Intra-cortical source activity differences between classes

Separate analyses of datasets, as well as the conjunction analysis revealed significant voxel-wise differences between the mean intra-cortical instantaneous amplitudes of the four EEG microstate classes in the four EEG frequency bands. In the following, the results of the conjunction analysis will be described.

Significant differences were observed for all four EEG frequency bands: delta, theta, alpha, and beta (see Inline Supplementary Figures 2 to 5). However, they were clearly dominated by the alpha frequency band as reflected by its' largest proportion of voxels differentially activated between classes compared to other bands (on average 34 % compared to 1 % in the delta, 3 % in the theta, and 3 % in the beta band, Table 1). Therefore, in the following, we focus on the sources in the alpha band.

---------- *Table 1 about here* ----------

---------- *Inline Supplementary Figure 1 about here* ----------

---------- *Inline Supplementary Figure 2 about here* ----------

---------- *Inline Supplementary Figure 3 about here* ----------

---------- *Inline Supplementary Figure 4 about here* ----------

Figures 2-4 illustrate these alpha band differences in six equidistant brain slices for classes A, B, and C compared to the other classes, respectively. EEG microstate class A was characterized by increased mean source strength in the alpha band in left posterior regions compared to classes B and D (Figure 2). EEG microstate class B was characterized by increased mean source strength in the alpha band in right posterior regions compared to class A and D (Figures 2 and 3). EEG microstate class C was characterized by increased mean source strength in the alpha band in large portions of the whole cortex, predominantly in the left temporal lobe compared to classes B and D, and right occipito-temporo-parietal areas compared to class A (Figures 2-4). EEG microstate class D was characterized by increased mean source strength in the alpha band in large portions of the whole cortex compared to classes A and B. We note that no other microstate class showed larger alpha source strength in any brain region than class C. Interestingly, the dorsolateral prefrontal cortex (BA 9) did not show any significant alpha source strength differences between classes.

In sum, microstate classes C and D were characterized by stronger mean source strength than classes A and B in wide-spread cortical regions, particularly in the right hemisphere compared to class A, and the left hemisphere compared to class B. Classes A and B were characterized by a lateralization difference. Class A showed increased left posterior and decreased right posterior alpha source strength compared to class B. Class C was characterized by increased occipital and left parietal alpha source strength compared to class D.

---------- *Figure 2 about here* ----------

---------- *Figure 3 about here* ----------

---------- *Figure 4 about here* ----------

3.3 Gravity centers and ROI-based means of intracortical source activities in the alpha band

Since the alpha EEG frequency band clearly appeared most decisive in determining the EEG microstate class topography, we applied two additional analyses to learn more about the spatial distribution of the alpha generators of the four classes.

Firstly, for each microstate class, we computed the center of gravity of the mean intra-cortical alpha source strength across participants, across the 6239 voxels. This analysis revealed four centers of activity for the four frequency bands. These centers of activity were all localized in the posterior cingulate cortex, consistently across the two datasets (dataset 1: mean MNI coordinates across classes x=0.45, y=-23.31, z=20.05, SD x=0.17, y=.12, z=0.11; dataset 2: mean coordinates across classes x=0.57, y=-24.66, z=17.61, SD x=0.15, y=.14, z=0.05). Theoretically, the center of gravity could lie outside the area of active neural sources. However, this was not the case in our datasets, in which for all microstate classes, voxels in the posterior cingulate cortex belonged to the third of voxels showing maximal source strength.

Secondly, we defined nine ROIs as follows. For each of the 6 comparisons between microstate classes in the alpha band, we identified all voxels significantly different between classes, separately for increases (occurred in 4 comparisons) and decreases (occurred in 5 comparisons). For each of these ROIs, we computed the mean instantaneous amplitude values across all voxels in the respective ROI. Their means across participants and the corresponding standard deviations are listed in Table 2. We note that for both Dataset 1 and Dataset 2, EEG microstate class B had higher right posterior compared to left posterior activity based on a contrast between activity means for ROIs 1 (left posterior) and 2 (right posterior) (Dataset 1: t=-2.75, p=.008; Dataset 2: t=-5.37, p<.001). There was no significant difference in activity levels between these two ROIs for microstate class A (Dataset 1: t=-0.34, p=.735; Dataset 2: t=1.22,

p=.228). Consequently, left-posterior intra-cortical alpha source strength was stronger in class A than class B (see Source Differences between Classes), and right-posterior activity in class B than A but only for class B a within-class-difference between mean left- and right-posterior source strength (based on the respective ROIs) was observed.

---------- *Table 2 about here* ----------

4. Discussion

The present study revealed consistent EEG frequency band-wise intra-cortical source strength differences between time periods associated with EEG microstate classes A, B, C, and D during resting across two independent datasets. Both datasets were obtained in healthy participants during eyes closed resting. The comparison of intra-cortical source strengths was performed by computing frequency-band specific instantaneous amplitudes in 6239 intra-cortical voxels. All possible combinations of classes were compared in the two datasets. Consistent differences across datasets were identified via a conjunction analysis.

4.1 Frequency-dependence of EEG microstate class topographies

In line with our hypothesis (see also Milz et al., 2016a), the spatial distribution and extent of intra-cortical source strength in the EEG alpha band predominantly determined whether a head-surface topography of class A, B, C, or D was induced. This was reflected by the large proportion of voxels differentially activated between microstate classes in this band (34 % on average across comparisons) compared to the negligible fractions in all other bands (< 5 % on average across comparisons). Previous studies had not been able to reveal conclusive results on the interrelationship between EEG microstate classes and spectral power characteristics (Britz et al., 2010; Musso et al., 2010). Our results showed that such interrelations can be reliably identified across datasets when location- / source- dependent power effects rather than global effects (e.g. derived from averages across channels) are investigated.

4.2 Intra-cortical sources of EEG microstate class topographies

The expected spatial differences in intra-cortical alpha source strength between classes were largely in agreement with our hypothesis (see also Milz et al., 2016a; Pascual-Marqui et al., 2014). EEG microstate class A showed increased left posterior alpha activity compared to classes B and D; EEG microstate class B showed increased right posterior alpha activity compared to classes A and D, and EEG microstate class C showed increased alpha activity in the anterior cingulate cortex (ACC) compared to all other classes.

Moreover, a center of gravity analysis revealed one main common source of intra-cortical alpha activity across microstate classes. This center was in the posterior cingulate cortex (PCC) for all four classes, and

consistently across the two datasets. A previous broad-band (2-20 Hz) source localization analysis also identified the PCC as a common center of activity to the four microstate classes (Pascual-Marqui et al., 2014). Our results indicate that this finding is likely accounted for by alpha activity.

However, contrary to our hypothesis, classes A and B did not show any location-specific alpha increases compared to class C. Instead, EEG microstate class C showed increased EEG alpha source activity compared to all other classes. These activity increases were observed in wide spread cortical regions beyond the ACC including the left and right posterior cortices. Therefore, our results further suggest that many brain regions beyond the default mode network are involved in the generation of the four EEG microstate class topographies.

4.3 EEG microstate analysis approach

We applied an EEG microstate analysis approach in which the EEG microstate class topographies were not computed based on the dataset at hand but were derived from reverence maps. This means that we did not recompute the four microstate classes based on the participants' EEG data in our datasets via the modified k-means clustering algorithm and subsequent first principal component-based mean computation procedures frequently applied in the past (e.g. Koenig et al., 1999; Nishida et al., 2013; Seitzman et al., 2016). Instead, we used the four normative class topographies published by Koenig et al. (2002) to identify the time periods within participants' EEGs corresponding to classes A, B, C, and D. The four normative classes were obtained from 496 healthy participants and are publicly available (www.github.com/keyinst/keypy). This approach was chosen for two reasons. Firstly, it allowed optimal comparison between the results derived from our two datasets. Secondly, it allows future studies to draw conclusions about the cortical regions involved in the generation of the normative map topographies rather than of the slightly varying topographies derived from the smaller datasets (N=61 and N=78) used in this study. Even though remarkably similar across many studies, at least some studies (e.g. Koenig et al., 1999; Nishida et al., 2013; Seitzman et al., 2016) report one or more of the four data-driven map topographies to deviate quite considerably from the normative maps (Koenig et al., 2002). The causes of such deviations and their effects on the EEG microstate class topographies' cortical sources remain to be investigated.

The disadvantage of our approach is that the percentage of variance explained by the four classes was slightly lower than the percentage reported in the literature. The explained variance in our datasets ranged from 65 % to 76 % (depending on whether we aimed to explain all EEG time frames or high signal-to-noise ratio GFP peak time frames only) as compared to more than 79 % in some (Kindler et al., 2011; Koenig et al., 1999; Koenig et al., 2002) but not all studies (e.g. Seitzman et al., 2016) that used a data-

driven microstate class computation approach. We assume that the unexplained variance reflects (1) the intermediary topographies that occur during transitions between microstate classes, which are topographical mixtures of the latter and typically shorter and of lower signal to noise ratio, (2) natural fluctuations in the exact topographical configuration of the four microstate classes across participants, and (3) systematic fluctuations of the topographical configuration of the four microstate classes which may be associated with a participants thinking modality (as for example reported by Milz et al 2016) or other factors that are yet to be identified.

We note that the choice to investigate exactly four EEG microstate classes rather than any lower or higher number of topographies was based on previous studies that identified four classes to be optimal based on a cross-validation criterion (e.g. Koenig et al., 1999) and a study that identified four normative EEG microstate classes based on a large sample of 469 healthy participants (Koenig et al., 2002). However, these studies investigated resting state EEG and used only a limited number of EEG recording channels. Both, the mental state and the degree of spatial resolution (which depends on the number of channels), may affect the number of microstate classes that optimally explain the variance of brain electric activity across time. Future studies must clarify whether this indeed is the case.

4.4 Impact of results

Our findings have fundamental implications on the interpretation of the brain functional dynamics reflected by the EEG microstates. They entail that time periods associated with the predominance of different EEG microstate classes are characterized by increased alpha source strength in specific brain regions. Alpha frequency oscillations reportedly exhibit inhibitory rather than excitatory brain activity, particularly in task-related brain areas that may include cortices involved in the processing of different sensory modalities or motor activities (Milz et al., 2016b; Pfurtscheller, 2003; Salenius et al., 1995; Slatter, 1960). Consequently, our results suggest that the EEG microstate dynamics may reflect systematic sequences of deactivation or inhibition in default mode network hubs (Pascual-Marqui et al., 2014) and additional brain areas rather than sequences of facilitation. Each class may represent a different attractor state that the brain repeatedly transitions into. The metabolic default mode network identified via fMRI likely reflects a temporally smoothed representation of these regular spatially-distributed states of inhibition or reduced cortical excitability.

Furthermore, our results have a fundamental impact on the interpretation of previous results retrieved from the EEG microstate analysis. For example, the apparent conflicting finding of increased prominence of class A reported during visualization, and class B during verbalization (Milz et al., 2015) and the associations of microstate classes A and B with metabolic networks associated with phonological and

visual processing, respectively (Britz et al., 2010) can now be resolved. Our results suggest that, in line with Britz et al. (2010), classes A and B are indeed associated with left and right posterior brain regions involved in phonological and visuo-spatial processing, respectively. However, increased prominence of classes A and B – if we accept the assumption that our broad alpha band reflects inhibitory activity in modality-related areas - reflect longer time periods during which the respective brain regions are inhibited rather than facilitated. Consequently, we found class A more prominently involved during visualization, and class B during verbalization as reported by Milz et al. (2016a).

Moreover, the previously reported increased prominence of class C during resting compared to tasks (Milz et al., 2016a; Seitzman et al., 2016) is no longer surprising when we consider that class C sources were characterized by increased alpha activity in 26 - 54 % of voxels and no decreases compared to all other classes. Decreased alpha activity, particularly in task-related areas, has frequently been reported in tasks compared to resting conditions (de Pesters et al., 2016; Pfurtscheller et al., 1996). This is also in line with the proposition made by Seitzman et al. (2016) that class C occurrence might be associated with the activity of a network that is more strongly activated when no explicit task is performed.

On a side note, descriptions of several samples described in the literature (e.g. Faber et al 2017; Schlegel et al 2011; Koenig et al 2002) and our results suggest that participants tend to spend most of their time during resting in the two microstate classes C and / or D rather than in A and / or B. That is, the topographies of either of the two classes of rather symmetric left- right- hemispheric distribution, and based on our results, increased alpha source strength, seem to be more prominent than the other two. This does not necessarily hold, however, for other states of consciousness (e.g. hypnosis: Katayama et al., 2007). Further research is needed to determine differing microstate class prominence patterns in different states or during task execution.

If EEG microstate class topographies were indeed driven by inhibitory alpha oscillations, as our results suggest, the question arises in favor of which brain regions these wide-spread alpha inhibitions might be taking place. Our analysis revealed only a very limited number of voxels significantly different in an EEG frequency band primarily associated with facilitation such as beta activity. The lack of significant differences in the beta band suggests that there may indeed be no specific brain regions consistently differentially facilitated between the four microstate classes or that such differences exist but involve brain regions of a strongly heterogeneous functional structure (Fehr, 2013) which would make it hard for group statistics to identify them. It remains to be investigated whether the same or very similar head-surface topographies would be retrieved, if the microstate analysis would be based on the alpha frequency band only rather than on the conventionally used broad frequency band of 2-20 Hz (Koenig et al., 2002; Lehmann et al., 2005; Pascual-Marqui et al., 2014).

The previous microstate literature suggested quite heterogenous functions for the four EEG microstate classes. They include associations with visual or verbal processing (Milz et al., 2016a), the default mode network Hz (Pascual-Marqui et al., 2014), task-negative and task-positive networks (Seitzman et al., 2016), reality testing (Kindler et al., 2011; Nishida et al., 2013; Rieger et al., 2016), autonomic, and attention-related processing (Britz et al., 2010).

Our results suggest that these heterogeneous associations may simply reflect the heterogeneity of functions of the many brain regions differentially involved in the generation of the four EEG microstate classes. Increased demands in one of these many functions may contribute to changes in duration and / or occurrence of particular EEG microstate classes in varying degrees.

5. Conclusions

The present study revealed that the intracortical strength and spatial distribution of intra-cortical alpha oscillations predominantly determine whether a head-surface topography of EEG microstate class A, B, C, or D is induced. EEG microstate class C was characterized by stronger alpha activity compared to all other classes in large portions of the cortex. Class A was associated with stronger left posterior alpha activity than classes B and D, and class B with stronger right posterior alpha than A and D.

Previous results already indicated that the EEG microstate dynamics reflect a fundamental mechanism of the human brain. These dynamics are characterized by systematic transitions between four head-surface topographies, the EEG microstate classes. Different patterns of transitions were associated with different mental states in health and disease. Our results show that these dynamic topographical changes are driven by intra-cortical alpha oscillations likely reflecting decreased cortical excitability. Thus, we propose that the EEG microstate class dynamics reflect systematic transitions between four global attractor states that are characterized by selective inhibition of specific intra-cortical regions.

6. Acknowledgements

This research did not receive any specific grant from funding agencies in the public, commercial, or not-for-profit sectors.

7. References

Andreou, C., Faber, P.L., Leicht, G., Schoettle, D., Polomac, N., Hanganu-Opatz, I.L., Lehmann, D., Mulert, C., 2014. Resting-state connectivity in the prodromal phase of schizophrenia: insights from EEG microstates. Schizophrenia Research 152, 513-520.

Britz, J., Van De Ville, D., Michel, C.M., 2010. BOLD correlates of EEG topography reveal rapid resting-state network dynamics. Neuroimage 52, 1162-1170.

Bruns, A., 2004. Fourier-, Hilbert-and wavelet-based signal analysis: are they really different approaches? Journal of neuroscience methods, 137(2), 321-332.

Brodbeck, V., Kuhn, A., von Wegner, F., Morzelewski, A., Tagliazucchi, E., Borisov, S., Michel, C.M., Laufs, H., 2012. EEG microstates of wakefulness and NREM sleep. Neuroimage 62, 2129-2139.

Chatrian, G., Lettich, E., Nelson, P., 1985. Ten percent electrode system for topographic studies of spontaneous and evoked EEG activities. American Journal of EEG technology 25, 83-92.

de Pesters, A., Coon, W., Brunner, P., Gunduz, A., Ritaccio, A., Brunet, N., de Weerd, P., Roberts, M., Oostenveld, R., Fries, P., 2016. Alpha power indexes task-related networks on large and small scales: A multimodal ECoG study in humans and a non-human primate. Neuroimage 134, 122-131.

Faber, P., Lehmann, D., Milz, P., Travis, F., Parim, N., 2014. EEG microstates differ between transcending and mind wandering. ZNZ Symposium 2014, Zurich.

Faber, P., Milz, P., Anderer, P., Reininghaus, E., Mörkl, S., Blesl, C., Wurm, W., Holl, A.K., Kapfhammer, H.-P., Saletu, B., Saletu-Zyhlarz, G.M., Kochi, K., Painold, A., in preparation. EEG macrostate and microstate characteristics in Huntington‘s Disease.

Faber, P.L., Lehmann, D., Barendregt, H., Kaelin, M., Gianotti, L.R., 2005. Increased duration of EEG microstates during meditation. Brain Topography 18, 131.

Fehr, T., 2013. A hybrid model for the neural representation of complex mental processing in the human brain. Cognitive Neurodynamics 7, 89-103.

Friston, K.J., Holmes, A.P., Price, C., Büchel, C., Worsley, K., 1999. Multisubject fMRI studies and conjunction analyses. Neuroimage 10, 385-396.

Goldberger, A.L., Amaral, L.A., Glass, L., Hausdorff, J.M., Ivanov, P.C., Mark, R.G., Mietus, J.E., Moody, G.B., Peng, C.-K., Stanley, H.E., 2000. Physiobank, physiotoolkit, and physionet. Circulation 101, e215-e220.

Katayama, H., Gianotti, L.R., Isotani, T., Faber, P.L., Sasada, K., Kinoshita, T., Lehmann, D., 2007. Classes of multichannel EEG microstates in light and deep hypnotic conditions. Brain Topography 20, 7-14.

Khanna, A., Pascual-Leone, A., Farzan, F., 2014. Reliability of resting-state microstate features in electroencephalography. Plos One 9, e114163.

Khanna, A., Pascual-Leone, A., Michel, C.M., Farzan, F., 2015. Microstates in resting-state EEG: current status and future directions. Neuroscience & Biobehavioral Reviews 49, 105-113.

Kindler, J., Hubl, D., Strik, W., Dierks, T., Koenig, T., 2011. Resting-state EEG in schizophrenia: auditory verbal hallucinations are related to shortening of specific microstates. Clinical Neurophysiology 122, 1179-1182.

Koenig, T., 2016. State dependent information processing, microstates and schizophrenia. International Journal of Psychophysiology 108, 12-13.

Koenig, T., Brandeis, D., 2016. Inappropriate assumptions about EEG state changes and their impact on the quantification of EEG state dynamics. Neuroimage 125, 1104-1106.

Koenig, T., Lehmann, D., Merlo, M.C., Kochi, K., Hell, D., Koukkou, M., 1999. A deviant EEG brain microstate in acute, neuroleptic-naive schizophrenics at rest. European Archives of Psychiatry and Clinical Neuroscience 249, 205-211.

Koenig, T., Prichep, L., Lehmann, D., Sosa, P.V., Braeker, E., Kleinlogel, H., Isenhart, R., John, E.R., 2002. Millisecond by millisecond, year by year: normative EEG microstates and developmental stages. Neuroimage 16, 41-48.

Kubicki, S., Herrmann, W.M., Fichte, K., Freund, G., 1979. Reflections on the topics: EEG frequency bands and regulation of vigilance. Pharmakopsychiatry Neuropsychopharmakology 12, 237-245.

Lehmann, D., 1990. Brain electric microstates and cognition: the atoms of thought. Machinery of the Mind. Springer, pp. 209–224.

Lehmann, D., 1993. Psychiatry and Microstates of the Brain's Electric Field: Towards the "Atoms of Thought and Emotion". Imaging of the Brain in Psychiatry and Related Fields. Springer, pp. 215-222.

Lehmann, D., Faber, P.L., Galderisi, S., Herrmann, W.M., Kinoshita, T., Koukkou, M., Mucci, A., Pascual-Marqui, R.D., Saito, N., Wackermann, J., 2005. EEG microstate duration and syntax in acute, medication-naive, first-episode schizophrenia: a multi-center study. Psychiatry Research: Neuroimaging 138, 141-156.

Lehmann, D., Ozaki, H., Pal, I., 1987. EEG alpha map series: brain micro-states by space-oriented adaptive segmentation. Electroencephalography and Clinical Neurophysiology 67, 271-288.

Lehmann, D., Pascual-Marqui, R.D., Michel, C., 2009. EEG microstates. Scholarpedia 4, 7632.

Lehmann, D., Pascual-Marqui, R.D., Strik, W.K., Koenig, T., 2010. Core networks for visual-concrete and abstract thought content: A brain electric microstate analysis. Neuroimage 49, 1073-1079.

Lehmann, D., Skrandies, W., 1980. Reference-free identification of components of checkerboard-evoked multichannel potential fields. Electroencephalography and Clinical Neurophysiology 48, 609-621.

Marple, L., 1999. Computing the discrete-time" analytic" signal via FFT. IEEE Transactions on Signal Processing 47, 2600-2603.

Mégevand, P., Quairiaux, C., Lascano, A.M., Kiss, J.Z., Michel, C.M., 2008. A mouse model for studying large-scale neuronal networks using EEG mapping techniques. Neuroimage 42, 591-602.

Michel, C., Brandeis, D., Koenig, T., 2009. Electrical neuroimaging in the time domain. In: Michel, C., Koenig, T., Brandeis, D., Gianotti, L., Wackermann, J. (Eds.), Electrical Neuroimaging. Cambridge University Press, Cambridge, pp. 111–143.

Milz, P., 2016. Keypy–An open source library for EEG microstate analysis. European Psychiatry 33, S493.

Milz, P., Faber, P., Lehmann, D., Koenig, T., Kochi, K., Pascual-Marqui, R., 2016a. The functional significance of EEG microstates—associations with modalities of thinking. Neuroimage 125, 643-656.

Milz, P., Pascual-Marqui, R.D., Lehmann, D., Faber, P.L., 2016b. Modalities of Thinking: State and Trait Effects on Cross-Frequency Functional Independent Brain Networks. Brain Topography 29, 477-490.

Musso, F., Brinkmeyer, J., Mobascher, A., Warbrick, T., Winterer, G., 2010. Spontaneous brain activity and EEG microstates. A novel EEG/fMRI analysis approach to explore resting-state networks. Neuroimage 52, 1149-1161.

Nichols, T., Brett, M., Andersson, J., Wager, T., Poline, J.-B., 2005. Valid conjunction inference with the minimum statistic. Neuroimage 25, 653-660.

Nichols, T.E., & Holmes, A.P., 2002. Nonparametric permutation tests for functional neuroimaging: a primer with examples. Human brain mapping 15(1), 1-25.

Niedermeyer, E., da Silva, F.L., 2005. Electroencephalography: basic principles, clinical applications, and related fields. Lippincott Williams & Wilkins.

Nishida, K., Morishima, Y., Yoshimura, M., Isotani, T., Irisawa, S., Jann, K., Dierks, T., Strik, W., Kinoshita, T., Koenig, T., 2013. EEG microstates associated with salience and frontoparietal networks in frontotemporal dementia, schizophrenia and Alzheimer's disease. Clinical Neurophysiology 124, 1106-1114.

Nuwer, M.R., 1987. Recording electrode site nomenclature. Journal of Clininical Neurophysiology 4, 121-133.

Pascual-Marqui, R.D., 2007. Discrete, 3D distributed, linear imaging methods of electric neuronal activity. Part 1: exact, zero error localization. arXiv preprint arXiv:0710.3341.

Pascual-Marqui, R.D., Lehmann, D., Faber, P., Milz, P., Kochi, K., Yoshimura, M., Nishida, K., Isotani, T., Kinoshita, T., 2014. The resting microstate networks (RMN): cortical distributions, dynamics, and frequency specific information flow. arXiv preprint arXiv:1411.1949.

Pascual-Marqui, R.D., Michel, C.M., Lehmann, D., 1995. Segmentation of brain electrical activity into microstates: model estimation and validation. Biomedical Engineering, IEEE Transactions on 42, 658-665.

Pedroni, A., Gianotti, L.R., Koenig, T., Lehmann, D., Faber, P., Knoch, D., 2016. Temporal characteristics of EEG microstates mediate trial-by-trial risk taking. Brain Topography, 1-11.

Pfurtscheller, G., 2003. Induced oscillations in the alpha band: functional meaning. Epilepsia 44, 2-8.

Pfurtscheller, G., Stancak, A., Neuper, C., 1996. Event-related synchronization (ERS) in the alpha band—an electrophysiological correlate of cortical idling: a review. International Journal of Psychophysiology 24, 39-46.

Pipinis, E., Melynyte, S., Koenig, T., Jarutyte, L., Linkenkaer-Hansen, K., Ruksenas, O., Griskova-Bulanova, I., 2016. Association Between Resting-State Microstates and Ratings on the Amsterdam Resting-State Questionnaire. Brain Topography, 1-4.

Poularikas, A.D., 1998. Handbook of formulas and tables for signal processing. CRC Press.

Raichle, M.E., MacLeod, A.M., Snyder, A.Z., Powers, W.J., Gusnard, D.A., Shulman, G.L., 2001. A default mode of brain function. Proceedings of the National Academy of Sciences USA 98, 676-682.

Rieger, K., Hernandez, L.D., Baenninger, A., Koenig, T., 2016. 15 years of microstate research in schizophrenia–where are we? A meta-analysis. Frontiers in Psychiatry 7.

Salenius, S., Kajola, M., Thompson, W.L., Kosslyn, S., Hari, R., 1995. Reactivity of magnetic parieto-occipital alpha rhythm during visual imagery. Electroencephalogrography & Clinical Neurophysiology 95, 453-462.

Schalk, G., McFarland, D.J., Hinterberger, T., Birbaumer, N., Wolpaw, J.R., 2004. BCI2000: a general-purpose brain-computer interface (BCI) system. IEEE Transactions on biomedical engineering 51, 1034-1043.

Schlegel, F., Lehmann, D., Faber, P.L., Milz, P., Gianotti, L.R., 2012. EEG microstates during resting represent personality differences. Brain Topography 25, 20-26.

Seitzman, B.A., Abell, M., Bartley, S.C., Erickson, M.A., Bolbecker, A.R., Hetrick, W.P., 2016. Cognitive manipulation of brain electric microstates. Neuroimage.

Slatter, K.H., 1960. Alpha rhythms and mental imagery. Electroencephalogragraphy & Clinical Neurophysiology 12, 851-859.

Strelets, V., Faber, P., Golikova, J., Novototsky-Vlasov, V., Koenig, T., Gianotti, L., Gruzelier, J., Lehmann, D., 2003. Chronic schizophrenics with positive symptomatology have shortened EEG microstate durations. Clinical Neurophysiology 114, 2043-2051.

Tomescu, M.I., Rihs, T.A., Becker, R., Britz, J., Custo, A., Grouiller, F., Schneider, M., Debbané, M., Eliez, S., Michel, C.M., 2014. Deviant dynamics of EEG resting state pattern in 22q11.2 deletion syndrome adolescents: A vulnerability marker of schizophrenia? Schizophrenia Research 157, 175-181.

Tsuno, N., Shigeta, M., Hyoki, K., Kinoshita, T., Ushijima, S., Faber, P.L., Lehmann, D., 2002. Spatial organization of EEG activity from alertness to sleep stage 2 in old and younger subjects. Journal of Sleep Research 11(1), 43-51.

Wackermann, J., Lehmann, D., Michel, C., Strik, W., 1993. Adaptive segmentation of spontaneous EEG map series into spatially defined microstates. International Journal of Psychophysiology 14, 269-283.

Figure Legends

Figure 1. The head-surface topographies of the four normative EEG microstate classes identified by Koenig et al. (2002) based on 496 participants. Positive electric potential values are depicted in red, negative electrode potential values are depicted in blue. Note that, in the EEG microstate analysis of spontaneous EEG, the spatial distribution of the potential values is the crucial parameter; polarity is disregarded.

Figure 2. Intra-cortical alpha (8.5-12 Hz) activity differences between EEG microstate class A and classes B, C, and D. Equidistant horizontal slices from z=-34 to 45 (MNI coordinates). Significant voxels ($p<.001$, uncorrected) are depicted in red (positive values) and blue (negative values). The number of voxels involved in significant alpha increases (pos) and decreases (neg) between classes are denoted separately for the left (LH) and right (RH) hemisphere.

Figure 3. Intra-cortical alpha (8.5-12 Hz) activity differences between EEG microstate class B and classes C and D (for details see Figure 2).

Figure 4. Intra-cortical alpha (8.5-12 Hz) activity differences between EEG microstate class C and D (for details see Figure 2).

Supplementary Figure Legends

Inline Supplementary Figure 1. Glass-brain views (top, left side, rear) of the eLORETA voxels significantly different ($p<.001$ uncorrected) between the four EEG microstate classes in the delta EEG frequency band. Positive values are depicted in red, negative values in blue.

Inline Supplementary Figure 2. Glass-brain views (top, left side, rear) of the eLORETA voxels significantly different ($p<.001$ uncorrected) between the four EEG microstate classes in the theta EEG frequency band. Positive values are depicted in red, negative values in blue.

Inline Supplementary Figure 3. Glass-brain views (top, left side, rear) of the eLORETA voxels significantly different ($p<.001$ uncorrected) between the four EEG microstate classes in the alpha EEG frequency band. Positive values are depicted in red, negative values in blue.

Inline Supplementary Figure 4. Glass-brain views (top, left side, rear) of the eLORETA voxels significantly different ($p<.001$ uncorrected) between the four EEG microstate classes in the beta EEG frequency band. Positive values are depicted in red, negative values in blue.

Tables

Table 1. Proportion of the 6239 voxels significantly different in activity (mean instantaneous amplitudes) between EEG microstate classes for the four EEG frequency bands delta through beta.

EEG frequency band	A vs. B	A vs. C	A vs. D	B vs. C	B vs. D	C vs. D
delta	0 %	2 %	1 %	2 %	0 %	1 %
theta	2%	4%	1%	7%	2%	0%
alpha	30%	46%	24%	54%	24%	26%
beta	2%	1%	4%	3%	2%	3%

Table 2. Mean and standard deviation (in brackets) of mean source activity (instantaneous amplitudes of current density in $\mu A/mm^2$) across voxels in 9 Regions of Interests (ROIs) across all participants. ROIs were derived based on all voxels significantly increased or decreased between classes of the 6 comparisons depicted in Figures 2-4. ROI 1: class A > B, ROI 2: class A < B; ROI 3: class A < C; ROI 4: class A > D; ROI 5: class A < D; ROI 6: class B < C; ROI 7: class B > D; ROI 8: class B < D; ROI 9: class C > D.

		Dataset 1				Dataset 2			
ROI	Region	Class A	Class B	Class C	Class D	Class A	Class B	Class C	Class D
ROI 1	left posterior	0.25 (0.07)	0.24 (0.07)	0.25 (0.07)	0.24 (0.07)	0.28 (0.15)	0.27 (0.14)	0.29 (0.16)	0.28 (0.14)
ROI 2	right posterior	0.24 (0.08)	0.26 (0.08)	0.26 (0.08)	0.26 (0.09)	0.29 (0.15)	0.30 (0.16)	0.31 (0.17)	0.31 (0.17)
ROI 3	wide-spread	0.21 (0.06)	0.22 (0.06)	0.22 (0.06)	0.22 (0.06)	0.26 (0.12)	0.26 (0.13)	0.28 (0.14)	0.27 (0.14)
ROI 4	left posterior	0.35 (0.10)	0.34 (0.10)	0.36 (0.09)	0.35 (0.09)	0.29 (0.15)	0.28 (0.14)	0.30 (0.16)	0.29 (0.15)
ROI 5	wide-spread	0.21 (0.07)	0.22 (0.07)	0.23 (0.07)	0.23 (0.08)	0.27 (0.14)	0.29 (0.15)	0.30 (0.16)	0.29 (0.16)
ROI 6	wide-spread	0.21 (0.05)	0.21 (0.05)	0.22 (0.06)	0.21 (0.06)	0.24 (0.11)	0.24 (0.11)	0.25 (0.12)	0.25 (0.12)
ROI 7	right posterior	0.27 (0.08)	0.28 (0.09)	0.28 (0.08)	0.27 (0.09)	0.32 (0.18)	0.33 (0.19)	0.33 (0.19)	0.32 (0.18)
ROI 8	wide-spread	0.19 (0.05)	0.19 (0.05)	0.20 (0.05)	0.20 (0.05)	0.24 (0.11)	0.24 (0.11)	0.26 (0.13)	0.25 (0.12)
ROI 9	wide-spread	0.24 (0.06)	0.23 (0.06)	0.24 (0.06)	0.24 (0.06)	0.26 (0.13)	0.26 (0.13)	0.28 (0.15)	0.26 (0.13)

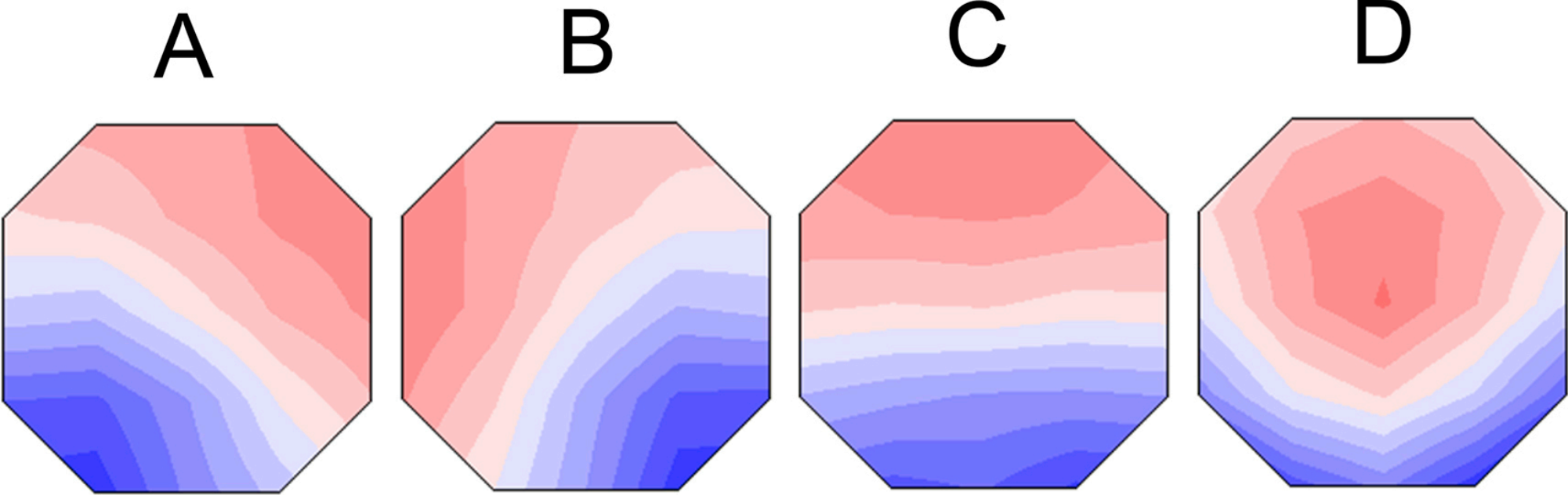
A
B
C
D

Alpha activity differences of class A

compared to class B

Top view

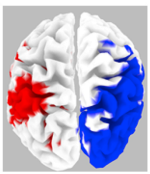

Horizontal slices

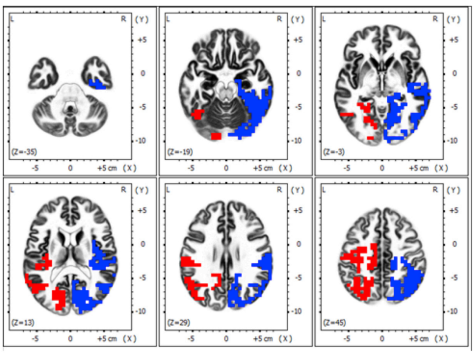

# voxels	LH	RH
pos	595	0
neg	0	1247

compared to class C

Top view

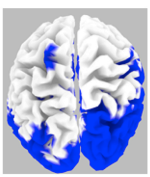

Horizontal slices

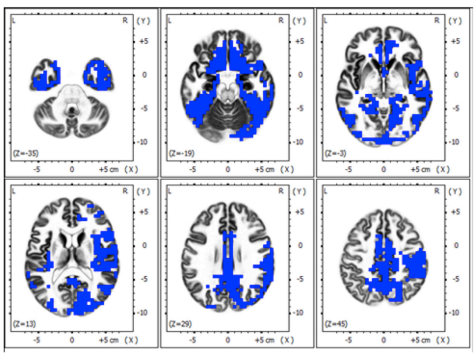

# voxels	LH	RH
pos	0	0
neg	838	1931

compared to class D

Top view

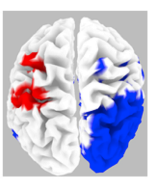

Horizontal slices

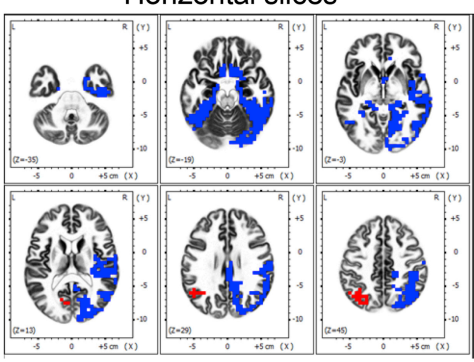

# voxels	LH	RH
pos	104	0
neg	172	1236

Positive values Negative values

Alpha activity differences of class B

compared to class C

Top view

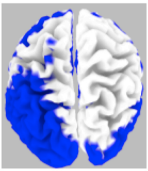

Horizontal slices

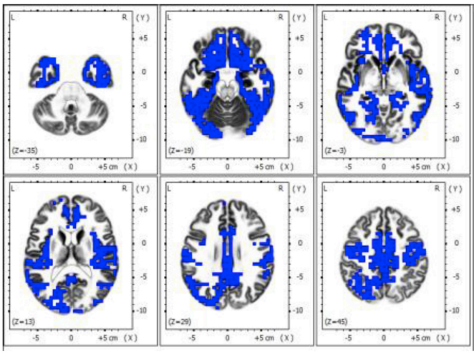

	# voxels	
	LH	RH
pos	0	0
neg	1800	1448

compared to class D

Top view

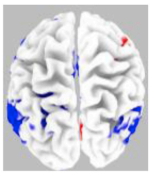

Horizontal slices

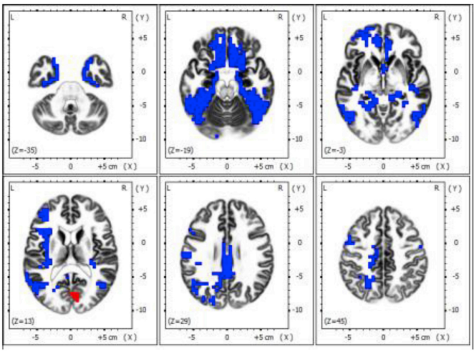

	# voxels	
	LH	RH
pos	0	29
neg	890	510

Positive values Negative values

Alpha activity differences of class C compared to class D

Top view

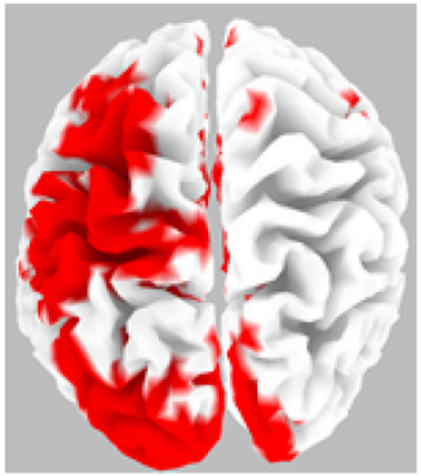

Horizontal slices

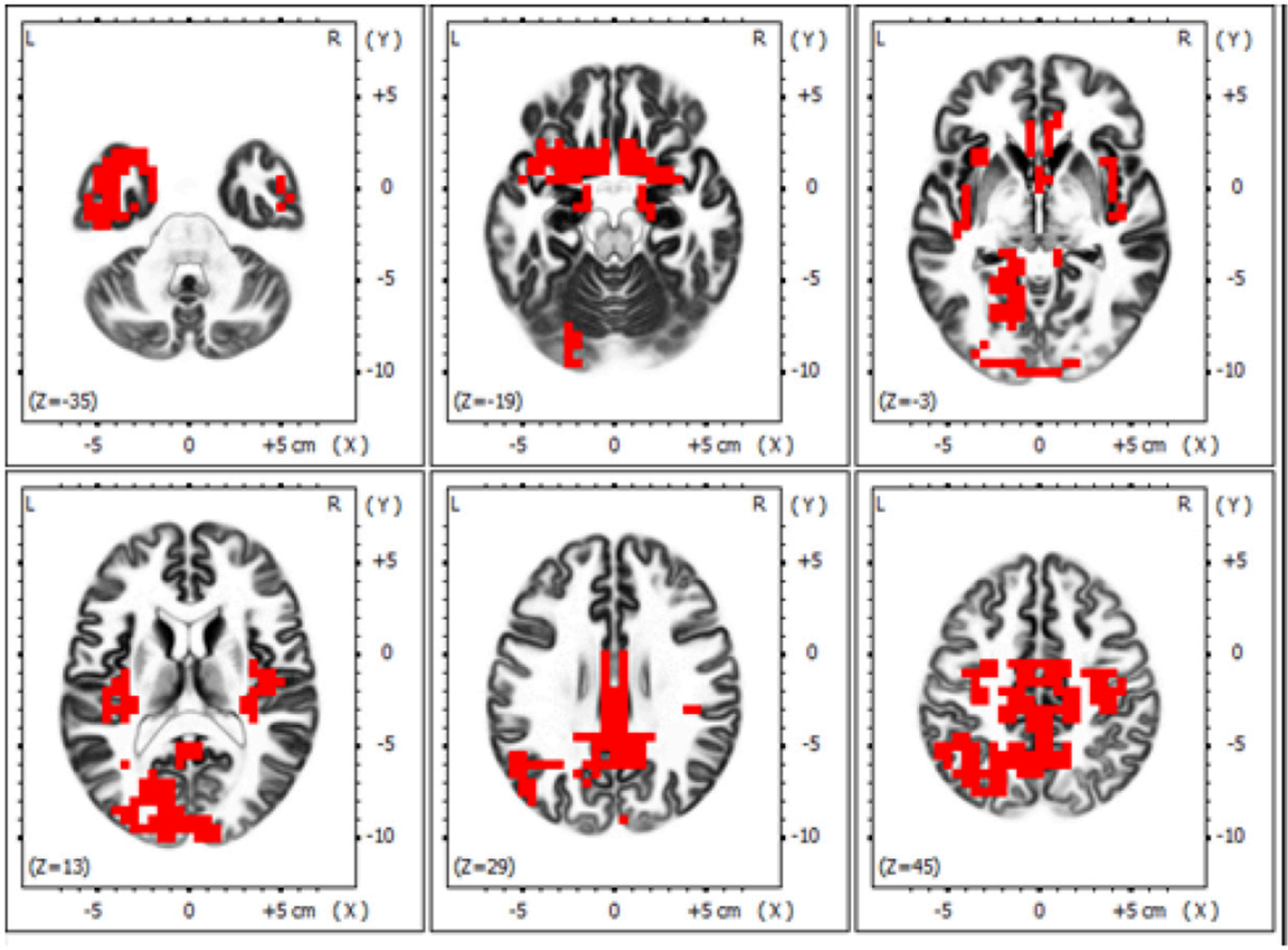

voxels

	LH	RH
pos	1070	457
neg	0	0

Positive values

Negative values